Second-sound attenuation in a supercritical counterflow jet*

Glenn A. Laguna
California Institute of Technology, Pasadena, California 91109
(Received 19 May 1975)

The attenuation of a beam of high-frequency second sound traversing a counterflow jet in liquid helium has been measured in the temperature range 1.6–2.06°K. Combined use of thin-film superconducting thermometers with specially developed low-noise amplifiers allowed resolution of the second-sound amplitude to better than one part in 10^8°K. The additional attenuation due to the jet was found to be less than 10% of the predicted value using the theory of mutual friction in a supercritical counterflow, and consistent with the result of earlier temperature-gradient and ion-beam attenuation measurements.

I. INTRODUCTION

Experiments published in recent years indicate that there may be a problem with the applicability of the idea of mutual friction to a counterflow jet in liquid helium. It is well established that mutual friction in a wide counterflow channel leads to both a temperature gradient proportional to the third power of the heat flux and to an additional attenuation of second sound.[1] However, application of these results to the jet which was observed by Kapitza[2] to emerge from the mouth of a counterflow channel seems to lead to a contradiction with the accepted theory of mutual friction.

The counterflow jet is shown schematically in Fig. 1. The two-fluid model would identify the effluent as normal fluid while the orifice represents a sink for the superfluid. The nozzle and orifice are regions of highest heat flux, therefore also the region of highest normal fluid velocity since the heat flux is given by

$$\vec{q} = \rho s T \vec{v}_n . \tag{1}$$

Kapitza observed that the jet spreads less than a turbulent jet, therefore the region of high normal fluid velocity extends far into the helium bath. If the superfluid is in sink flow, then $v_s \ll v_n$ except close to the orifice, so that in the jet

$$\vec{w} = \vec{v}_n - \vec{v}_s \simeq \vec{v}_n . \tag{2}$$

Therefore, with the mutual friction force in the Gorter-Mellink[3] form,

$$\vec{F}_{ns} = A(T)\rho_n \rho_s w^2 \vec{w} , \tag{3}$$

one should observe a temperature grandient extending well beyond the orifice.

The temperature gradient in an axisymmetric jet was measured by Dimotakis and Broadwell[4] by traversing a small carbon thermometer along the jet axis. A similar measurement done on the jet used in this experiment, which had a length-to-width ratio of 4, is shown in Fig. 2. The temperature gradient exactly followed the law

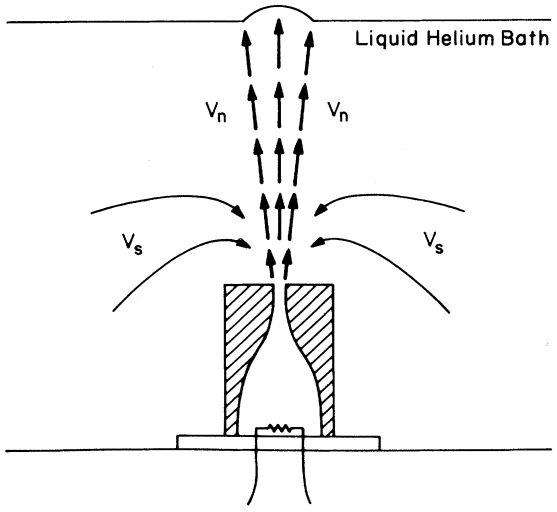

FIG. 1. Counterflow jet.

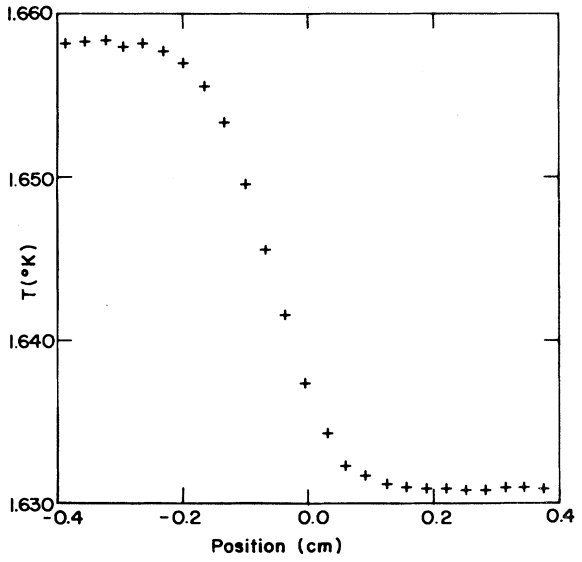

FIG. 2. Temperature gradient measured in the jet. The exit plane is at 0.0 and positive positions are in the free jet. Heat flux = 3.46 W/cm^2.

$$T = -b(T)q^3, \quad b(T) = A(T)[\rho_n/s(\rho_s sT)^3], \tag{4}$$

when the small carbon thermometer was within the straight section of the nozzle. However, the gradient disappeared within one diameter of the orifice. This is a very surprising result in view of the geometry independence of the gradient coefficient $b(T)$. One can only conclude that the Gorter-Mellink force is not active in the counterflow jet.

One possible explanation which was put forth was that in the jet $w = 0$, i.e., the superfluid is entrained by the normal fluid. Consideration of the resulting streamline pattern shows that there must be a stagnation point of the superfluid close to the orifice. However, Dimotakis and Broadwell showed that the temperature profile was self-similar for all bath temperatures and heat fluxes if plotted as a function of a reduced temperature,

$$\tau = (T - T_\infty)/\Delta T, \tag{5}$$

where T_∞ is the bath temperature and ΔT is the temperature difference across the nozzle. If superfluid entrainment was the explanation for the absence of a temperature gradient in the jet, then in order to preserve the streamline pattern entrainment of the superfluid would have to take place with the same efficiency while the relative velocity within the orifice varied over three orders of magnitude. Thus entrainment appears an improbable explanation for the temperature profile.

In 1968 Careri, Cerdonio, and Dupre[5] performed a different experiment which, in combination with Vinen's[6] model of mutual friction, leads to a contradiction with the Dimotakis-Broadwell result. Careri's experiment consisted of the observation of a beam of negative ions traversing the jet. The beam on the normal fluid downstream (hereafter called only downstream) side of the orifice was strongly attenuated at a critical heat flux, but the temperature difference across the orifice was still linear in the heat flux. Since negative ions are trapped by quantized vortices, the attenuation of the ion beam is a direct measure of the vorticity in the superfluid so that Careri's observation confirms the presence of vorticity in the normal fluid jet. If the mutual friction is caused by a random distribution of vorticity, as in the Vinen model, it is paradoxical that the jet has vorticity but the temperature gradient associated with the Gorter-Mellink force is absent.

In the present experiment an emitter and detector for second sound were placed in a Fabry-Perot-resonator configuration on the normal-fluid downstream side of the jet. The attenuation of the second-sound beam was measured as a function of the heat flux in the jet. If, as observed by Kapitza and by Dimotakis,[7] the jet does not spread, then zero attenuation would be consistent with the results of Dimotakis and Broadwell. If attenuation of the second sound was observed, this would confirm Careri's measurement and could be compared to Vinen's data for second-sound attenuation in wide counterflow channels.

II. EXPERIMENTAL APPARATUS

A. Counterflow jet

The counterflow jet is shown is Fig. 3. It is constructed of Lucite with a wall thickness of 0.32 cm. The heater at the base of the wide chamber is 25 Ω and is constructed of 0.0127-cm Evanohm wire. Uniform heat distribution over the bottom of the channel was ensured by plotting the heater in Cerelow.

The orifice is a slit 0.16 cm wide and 0.64 cm long. It is the only region of high heat flux. This shape was chosen for easier alignment of the second-sound beam with the jet, while the total area was dictated by the desire to produce heat fluxes comparable to previous experiments and still being able to maintain the bath temperature within the required limits.

B. Second-sound equipment

The second-sound emitter and detector are shown in Fig. 4. The emitter was a gold film less than 100 Å thick and $\frac{1}{2}$ cm^2 with 1500-Å-thick copper leads evaporated under high vacuum onto a glass

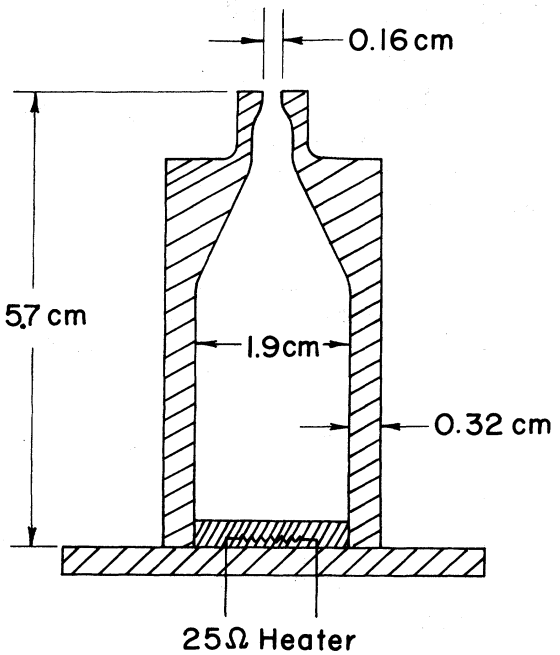

FIG. 3. Design details of the counterflow jet used in the present experiments.

microscope slide. Electrical contact to the copper was made with indium solder and a drop of silver-print paint. The resistance of the emitter was kept very close to 50 Ω at 4.2 °K to match the impedance of the subminiature coax, thereby reducing second-harmonic generation. Second sound was generated by Joule heating of the resistive gold film.

A superconducting thin film biased on its transition temperature served as the second-sound detector. When the film is fed with a constant current, the second-sound temperature fluctuations cause a fluctuating resistance of the film and therefore an oscillating voltage across it. The films were approximately 1000 Å of tin on 250 Å of gold. Leads were 1500 Å of pure tin which has a transition temperature of 3.72 °K and therefore is not sensitive to the temperature fluctuations of second sound. The sensitive area is the 1-mm-square flag-shaped region in the center.

The basic transition temperature of the film was set by the ratio of tin to gold, but this transition could be lowered by means of a magnetic field. In this way one film served as a detector over a wide temperature range. By optimizing the bias current, the detector efficiency could be made as high as 0.6 V/°K.

The second-sound cell served the dual purposes of holding the emitter and detector parallel and supporting the magnet which biased the detector. Provision was made for varying the emitter detector spacing from 4 mm to 1 cm. Alignment of the emitter and detector is by three set screws for each side arranged similar to a laser mirror mount, and was accomplished at room temperature by means of a helium-neon laser and an optical setup. Because the entire support structure is of the same material, there can be no differential contradiction so alignment at room tempera-

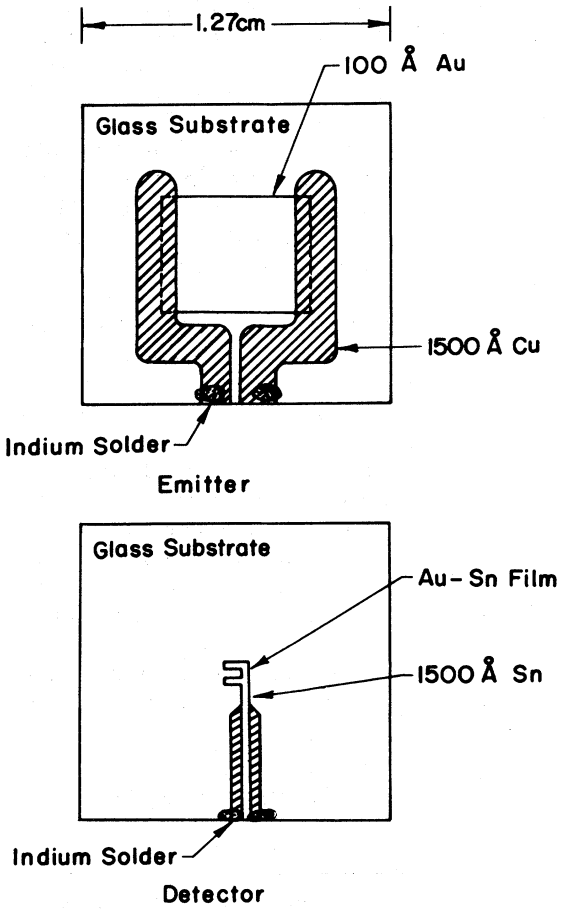

FIG. 4. Second-sound emitter and detector.

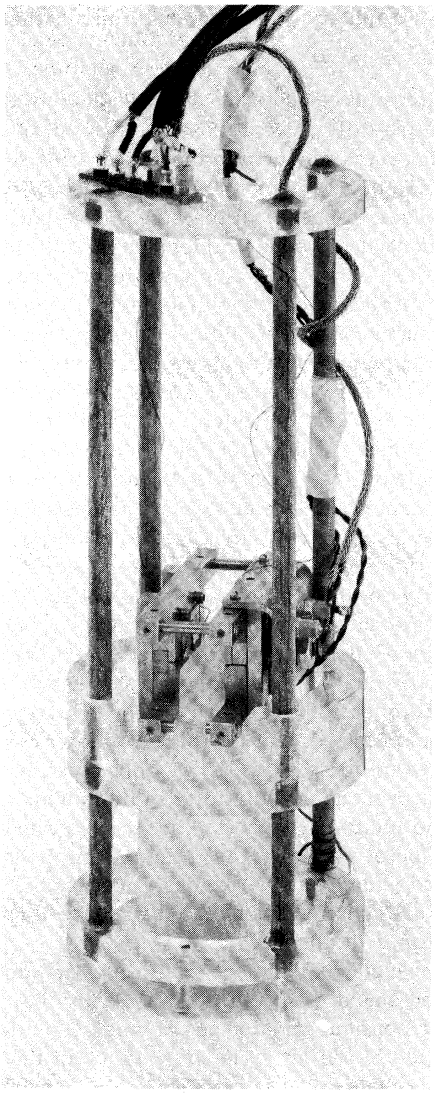

FIG. 5. Assembled counterflow jet and support structure with the second-sound cell.

ture is maintained at helium temperatures. The maxium misalignment was 0.15 deg, which corresponds to an alignment of better than 0.1λ for second-sound frequencies up to 1 MHz.

The entire assembly of the jet, second-sound cell, and supporting structure is shown in Fig. 5. Figure 6 shows a top view schematic, drawn to scale, of the orifice, emitter, and detector.

Temperature regulation was by means of regulation of the bath pressure using a condom regulator.[8] The pressure above the bath was monitored with a 100-mm full-scale Barocell pressure transducer and converted to temperature using the 1958 ^{4}He temperature scale. To maintain constant temperature for the duration of the experiment, it was necessary to maintain a constant heat input into the Dewar. This necessitated multiplexing between the jet heater and a ballast heater of approximately the same resistance wound around the base of the supporting structure. The maximum temperature drift, at low temperatures and high heat fluxes, was less than 0.3 mdeg. Therefore, at the working frequency of 100 kHz, the limitation imposed by temperature regulation was 0.1% of the attenuation due to the Gorter-Mellink force in a channel of comparable dimensions.

C. Electronics

A block diagram of the electronics for the generation and detection of second sound is shown in Fig. 7. At the heart of the emitter system is a General Radio 1310B sine-wave generator with a frequency range of 2 Hz–2 MHz and a short-term drift of 0.3 ppm over 10 min. This oscillator is capable of being synchronized to an external reference signal which was derived from the wave-analyzer beat-frequency oscillator (BFO) output. The BFO signal was converted to a square wave and its frequency digitally divided in half in a device labeled "Frequency DDT." This synchronized the oscillator to exactly half the center frequency of

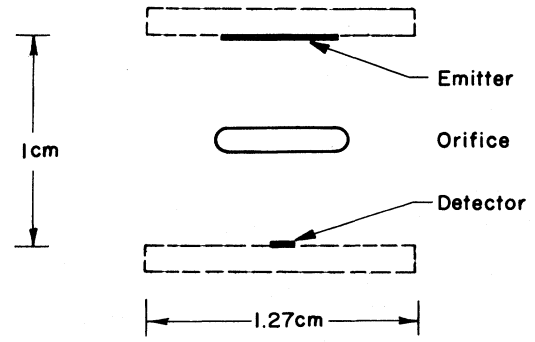

FIG. 6. Top-view schematic of the emitter, detector, and orifice geometry.

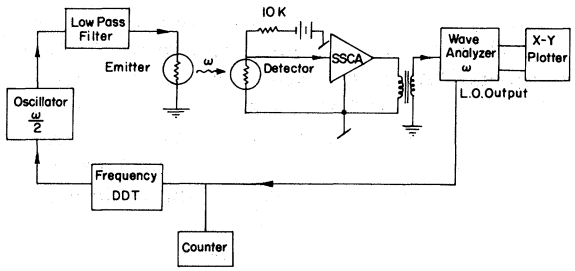

FIG. 7. Second-sound electronic instrumentation. DDT is a digital frequency divider. SSCA stands for small-signal current amplifier.

the wave-analyzer passband and also enabled the scanning local oscillator of the wave analyzer to sweep the second-sound frequency. This method of frequency division is digitally precise as compared to the usual frequency doubling by a nonlinear element which has a typical accuracy of about 1%.

The detector electronics consisted of a small signal current amplifier (SSCA) and wave analyzer. The amplifier had a bandwidth of 30 MHz with a noise figure of 3.3 nV/(Hz)$^{1/2}$, and served as a preamplifier. With detector efficiencies as high as 0.6 V/°K this current amplifier gives a signal-to-noise ratio of unity for 50-ndeg second-sound amplitudes. Minor changes in the electronics would improve this by a factor of 10 but amplifier noise did not represent a limitation in this measurement. The SSCA and the detector formed the low-level part of the signal detection system and so were provided with a separate ground.

The two wave analyzers used were a Hewlett-Packard model 3590A with 3594A sweeping local oscillator for frequencies below 600 kHz and a Hewlett-Packard Model 310A with 297A sweep drive for frequencies up to 1.2 MHz. These provided narrow-band filters and also the reference signal used to sweep the second-sound cavity through its resonance. Both analyzers provided a dc ramp proportional to the center frequency of the filter and a dc voltage proportional to the rms value of the signal component within the passband. The two outputs from the wave analyzer were fed into an X-Y plotter. Thus the wave analyzer generated a plot of second-sound amplitude vs frequency, i.e., the second-sound spectrum of the resonant cavity.

III. ATTENUATION MEASUREMENTS

A. Second-sound resonance technique

A traveling second-sound wave in the x direction can be represented as

$$e^{-\alpha x} e^{i\omega(t-x/u_2)}. \tag{6}$$

The second-sound resonator is ideally formed by an infinite-plane emitter with the detector being an infinite perfect reflector having a small sensing element in its center. The geometrical-optics approximation is valid here provided the second-sound wavelength is much smaller than the emitter dimensions. Notarys[9] found that his detectors exhibited negligible reflective loss even at high frequencies. If the power input per unit area to the emitter is $(Q/A)\cos\omega t$, then the amplitude at the detector will be

$$(\Delta T)_{ss} = \frac{Q}{A}\frac{1}{\rho c u_2} \times \frac{1}{[\cosh^2\alpha D - \cos^2(\omega D/u_2)]^{1/2}} \cos(\omega t - \varphi), \tag{7}$$

$$\varphi = \tan^{-1}[\coth\alpha D \tan(\omega D/u_2)]. \tag{8}$$

In this formula c is the heat capacity and D is the spacing between the emitter and detector.

A resonance condition is satisfied whenever

$$\omega D/u_2 = n\pi. \tag{9}$$

At a fixed temperature this can be accomplished by varying ω; however, it can also be accomplished by holding the frequency fixed and allowing the bath temperature to drift, thus changing u_2. The speed of second sound can therefore be measured at a fixed temperature by measuring the frequencies of two successive resonances, i.e.,

$$u_2 = (\omega_{n+1} - \omega_n)(D/\pi). \tag{10}$$

An expression for the attenuation can be derived from Eq. (7) by the expansion of $\cosh^2\alpha D$ for small argument and the expansion of $\cos^2(\omega D/u_2)$ near a resonance. By measuring the width $\Delta\omega$ of the resonance curve at $1/\sqrt{2}$ of the maximum height one finds for a frequency resonance

$$\alpha = \Delta\omega/2u_2 \quad (T \text{ constant}). \tag{11}$$

For a temperature resonance the expansions give

$$\alpha = \frac{\Delta T}{2}\frac{\omega}{u_2^2}\frac{du_2}{dT} \quad (\omega \text{ constant}). \tag{12}$$

If there is an additional attenuation $\Delta\alpha$ when the jet is turned on, then α in the above formulas is replaced by $\alpha+\Delta\alpha$. There is an easier way to get $\Delta\alpha$ provided α has already been measured. One can find $\Delta\alpha$ by a comparison of the height of the resonance peaks for the jet on and jet off, i.e.,

$$\frac{(\Delta T_{ss})_{on}}{(\Delta T_{ss})_{off}} = \left(\frac{\cosh^2\alpha D - 1}{\cosh^2(\alpha+\Delta\alpha)D - 1}\right)^{1/2}. \tag{13}$$

Expansion of the cosh terms gives

$$\Delta\alpha = \alpha\left(\frac{(\Delta T_{ss})_{off}}{(\Delta T_{ss})_{on}} - 1\right). \tag{14}$$

B. Data-taking procedure

This section is an outline of the basic experimental-run procedure for measuring the added attenuation of second sound due to the counterflow jet. The emitter detector spacing and distance from the orifice were fixed while the apparatus was at room temperature before a set of experimental runs.

At liquid-helium temperatures the run was started by setting the bath temperature using the condom regulator. The detector was then biased in the middle of its transition at that temperature by means of 10-turn potentiometer on the magnet current supply. A resonance peak was found by scanning the wave analyzer close to the desired operating frequency. Then the amplitude of the General Radio oscillator was adjusted so that the noise level was less than 1% of the second-sound amplitude on resonance. This could be accomplished with a power input less than 0.01 W/cm^2 into the emitter and it was experimentally verified that this caused no finite-amplitude effects or power broadening of the resonance.

Finally, the heat flux of the jet was set by adjusting the current into the ballast heater. The bath was allowed to reach its new equilibrium pressure, usually within a few milliTorr of the limited pressure and not enough to cause a change in the detector bias point. A frequency sweep was then made with the jet off. At the end of this sweep the sweeping local oscillator of the wave analyzer was returned to its starting point and the jet turned on. Although it took less than 2 sec for the jet to turn on, 30 sec usually elapsed between the off and on sweeps allowing the bath to come fully to equilibrium once again. A series of such runs

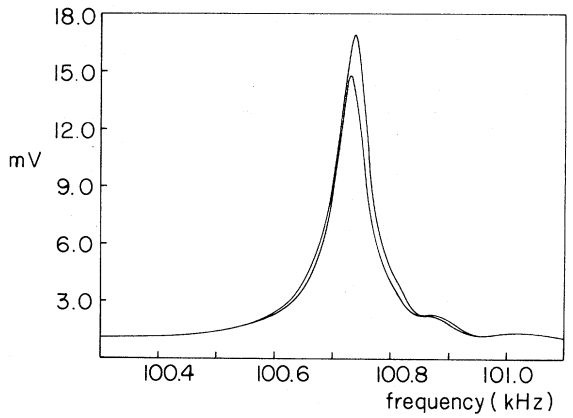

FIG. 8. Frequency resonance at $T = 2.06$ °K and heat flux of 1.23 W/cm^2. Upper trace is with the jet off and lower trace is with the jet on.

was made at each temperature with heat fluxes increasing from 0.3 W/cm^2 until it was no longer possible to maintain constant bath temperature. This occured at heat fluxes between 2.5 W/cm^2 at lower temperatures and 4 W/cm^2 at the highest temperature measured.

C. Discussion of experimental resonance curve

A typical experimental run at $T = 2.056$ °K is shown in Fig. 8. The higher trace was with the jet off and the lower trace with the jet on. For this run the resonant frequency was approximately 100.74 kHz and the heat flux at the orifice was 1.23 W/cm^2. The additional attenuation is quite noticeable.

There is a slight shift in frequency of about 10 Hz between the peaks with the jet on and the jet off. This was almost always present but not consistent in either size or direction, and was attributed mostly to the short-term drift of the wave-analyzer sweep oscillator.

Some justification is needed for measurements at frequencies as low as 100 kHz since non-negligible diffraction was observed at this frequency. Diffraction should not affect the relative attenuation measurements since the same loss of beam would be present both with the jet on and with the jet off. However, an experimental check was made just to be sure. The resonance curves were measured with the jet on and jet off at two frequencies, 100 and 250 kHz. From these measurements the relative attenuation was computed in two ways. First, the total attenuation was computed for each peak using the width at 0.707 of the maximum in Eq. (11). Subtraction then gave the additional attenuation with the jet on. In addition, the change in attenuation was computed from the ratio of the resonant amplitudes and bulk attenuation using Eq. (14). These four values of the additional attenuation were the same to within experimental accuracy, and this provides the justification for the 100-kHz measurements. It also shows that the additional attenuation due to the jet is independent of frequency.

It was found that for a given temperature and position downstream of the orifice, the additional attenuation ($\Delta\alpha$) versus the heat flux (q) fell on a straight line when plotted on logarithmic graph paper; i.e.,

$$\log(\Delta\alpha) = \log I + n\log q. \tag{15}$$

An example is shown in Fig. 9. Therefore, one can consider all of the data in the form

$$\Delta\alpha = Iq^n, \tag{16}$$

where I represents the additional attenuation due to the jet at a heat flux of 1 W/cm^2.

The measured values of I at 3.2 and 20 diameters downstream are shown in Figs. 10 and 11. A line which is the best polynomial fit to the data is also plotted.

For the 20-diameter measurements one straight line would not fit all the data on the log-log plot; however, the data at high heat fluxes and low heat fluxes could be fit separately by two straight lines of different slope and intercept. This possibly represents some type of a transition between two

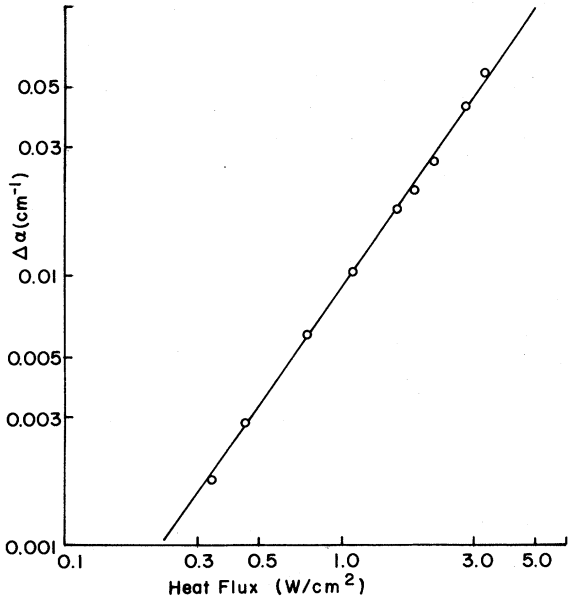

FIG. 9. Additional attenuation vs heat flux at $T = 1.623$ °K and 9.6 diameters downstream.

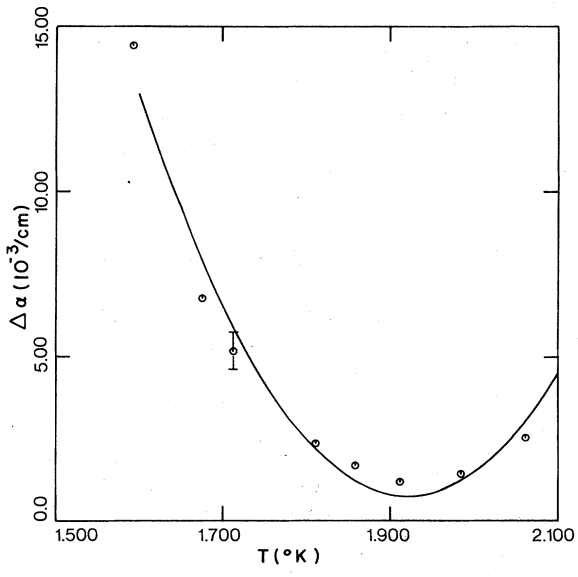

FIG. 10. Additional attenuation vs T for a heat flux of 1W/cm^2 at 3.2 diameters downstream.

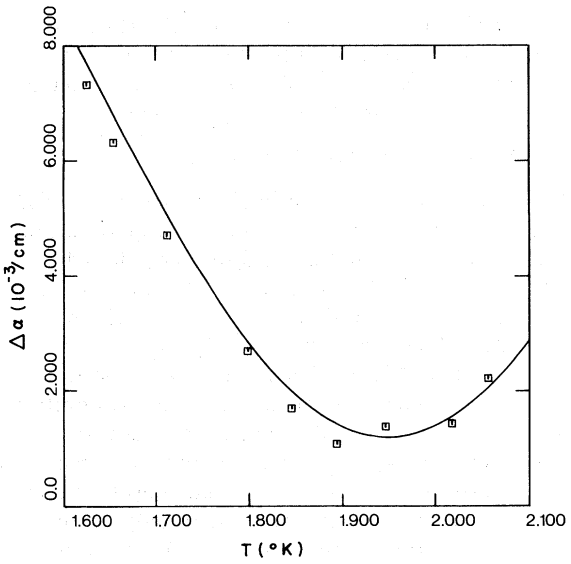

FIG. 11. Additional attenuation vs T for a heat flux of 1 W/cm^2 at 20 diameters downstream.

flow regimes. Figure 11 is the intercept values of the line which fit the higher-heat-flux data.

IV. RESULTS AND DISCUSSION

The experimental results are summarized by the plot of $\Delta\alpha/\alpha_{GM}$ vs T shown in Fig. 12. $\Delta\alpha$ is the change in attenuation for a heat flux of 1 W/cm^2. The quantity α_{GM} is the attenuation due to the Gorter-Mellink force which would be present for the same heat flux in a channel. Recall that this heat flux must be carried by the normal fluid in the jet. If the superfluid is not entrained by the normal fluid, and if the Gorter-Mellink force is a true volume force which acts in the absence of walls, then α_{GM} should also be the attenuation of second sound in the free jet.

There are several observations that can be made on the basis of Fig. 12. The observed attenuation is always less than 8% of the Gorter-Mellink attenuation, and $\Delta\alpha/\alpha_{GM}$ is clearly temperature dependent. In addition, the observed $\Delta\alpha$ follows a different power-law dependence on the heat flux than α_{GM}. The Gorter-Mellink attenuation is proportional to q^2 while the observed attenuation goes as q^n with $n = 1.3$–1.6.

The geometry dependence can be accounted for, to some extent, by spreading of the jet. The spreading would have to be considerably more than has been observed by Kapitza and by Dimotakis.[7] Because the length-to-width ratio of the jet is not large, the ordinary spreading relations for a plane turbulent jet are not entirely applicable, nor are those for an axisymmetric jet. Although all turbulent jets spread linearly with distance, the angle of spreading depends on the geometry. No geometric scaling can bring the observed attenuation into agreement with the attenuation in a channel because there is already a substantial difference at $x/d = \frac{1}{2}$, where the jet cannot have spread appreciably. Thus the observed attenuation cannot be due to mutual friction in the sense that this describes the temperature gradient in a channel. However, this conclusion does not shed any new light on how the mutual friction hypothesis is violated. The question of whether the superfluid is entrained by the normal fluid, or whether the Gorter-Mellink force acts only in the presence of walls is still unanswered.

The attenuation results are qualitatively consistent with both the axial-gradient measurements of Dimotakis and Broadwell and Careri's ion-beam attenuation measurements. Comparatively little attenuation of second sound was observed which would be expected from the lack of temperature gradient in the jet. The fact that some attenuation was observed indicates that the flow in the jet is inhomogeneous, thus confirming Careri's observation of ion-beam attenuation on the downstream side of his orifice. A further comparison with Careri's data does not seem possible. All of Careri's counterflow measurements were below 1.4 °K, and because of the small size of the orifice and low heat flux his Reynolds numbers were always below 1000. In particular, the Reynolds number based on normal fluid density

$$R_n = \rho_n d v_n/\eta \tag{17}$$

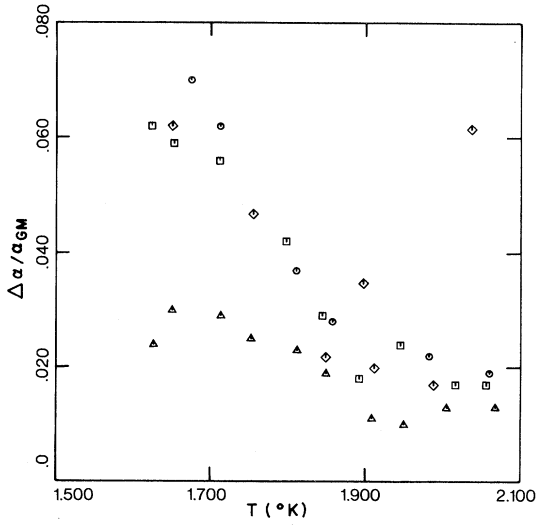

FIG. 12. Ratio of the measured attenuation at 1 W/cm^2 to attenuation predicted from the mutual-friction theory.

is only 20–30 at these low temperatures, compared with several thousand for the second-sound attenuation measurements. It is unclear how to find another dimensionless group to scale the data, or even if one can be found.

It is possible to make a quantitative comparison between the second-sound attenuation and temperature-gradient measurements. According to the mutual-friction theory, the temperature gradient can be related to the attenuation by using the equations

$$\nabla T = b(T) q^3, \quad \alpha_{GM} = c(T) q^2, \tag{18}$$

where $b(T)$ is given in Eq. (4) and

$$c(T) = A\rho / 2u_2(\rho_s s T)^2. \tag{19}$$

One finds that

$$\nabla T = \gamma(T) q \alpha_{GM}. \tag{20}$$

For comparison, the gradient is computed from the observed attenuation $\Delta\alpha$ instead of α_{GM}. As a typical example, $\nabla T = 6.66 \times 10^{-4}$°K/cm for a bath temperature at 1.6°, heat flux of 2.66 W/cm^2, and $\Delta\alpha$ measured at 9.6 diameters downstream. This is within the noise level of the carbon thermometer, i.e., such a gradient would be undetectable. The calculation illustrates the increased sensitivity of the second-sound attenuation compared to the gradient measurements.

The second-sound attenuation in the jet was observed to be frequency independent. If the attenuation is viewed as a scattering process due to inhomogeneities in the flow field, this would indicate that the second-sound wavelength is smaller than the length scale of the homogeneities responsible for the scattering. Both Kovasznay[10] and Schmidt[11] have observed frequency-independent scattering of ultrasonic waves in turbulent flows when the wavelength was less than the microscale of the turbulence. This condition was fulfilled in the second-sound-attenuation experiments, the wavelength being comparable to or slightly less than the microscale. It is possible that a calculation of the attenuation can be based on geometrical acoustics. This work is now in progress.

V. CONCLUSION

A technique for the use of high-frequency second sound to study the fluid mechanics of liquid helium has been developed and applied to study the additional attenuation of a second-sound beam traversing a supercritical counterflow jet. Although the attenuation of the beam was clearly measurable, it was less than 10% of that predicted by the mutual-friction theory and measured in a counterflow channel. The size of the attenuation is quantitatively consistent with earlier temperature-gradient measurements. This once again suggests that either the Gorter-Mellink force acts only in the presence of walls, or the relative velocity is nearly zero in the free jet.

The additional attenuation of second sound by the jet indicates that the flow is inhomogeneous, thus qualitatively confirming earlier investigators measurements of the ion-beam attenuation due to counterflow through an orifice. Frequency independence of the second-sound attenuation suggests that the inhomogeneities are larger than the second-sound wavelength. The attenuation vs temperature at various distances downstream from the orifice follow similar well-defined curves indicating that future experimental and theoretical study is warranted.

ACKNOWLEDGMENTS

The author would like to thank Professor Hans W. Liepmann, Dr. Paul Dimotakis, and Dr. James E. Broadwell for their suggestions concerning the experiment. He is also indebted to Dr. Harris Notarys and Dr. David Palmer for their instruction in thin film fabrication.

---

*Work supported by the Alfred P. Sloan Foundation and the Airforce Office of Scientific Research.

[1]W. F. Vinen, Proc. R. Soc. Lond. A 240, 114 (1957).
[2]P. L. Kapitza, J. Phys. USSR 5, 181 (1941).
[3]C. J. Gorter and J. H. Mellink, Physica 15, 285 (1949).
[4]P. E. Dimotakis and J. E. Broadwell, Phys. Fluids 16, 1787 (1973).
[5]G. Careri, M. Cerdonio, and F. Dupre, Phys. Rev. 167, 233 (1968).
[6]W. V. Vinen, Proc. R. Soc. Lond. A 242, 493 (1957).
[7]P. E. Dimotakis, Ph.D. thesis (California Institute of Technology, 1972) (unpublished).
[8]H. A. Notarys (private communication).
[9]H. A. Notarys, Ph.D. thesis (California Institute of Technology, 1964) (unpublished).
[10]Chih-Ming Ho and L. S. G. Kovasznay, report (unpublished).
[11]Dieter W. Schmidt, AGARD Report No. 461, 1963 (unpublished).

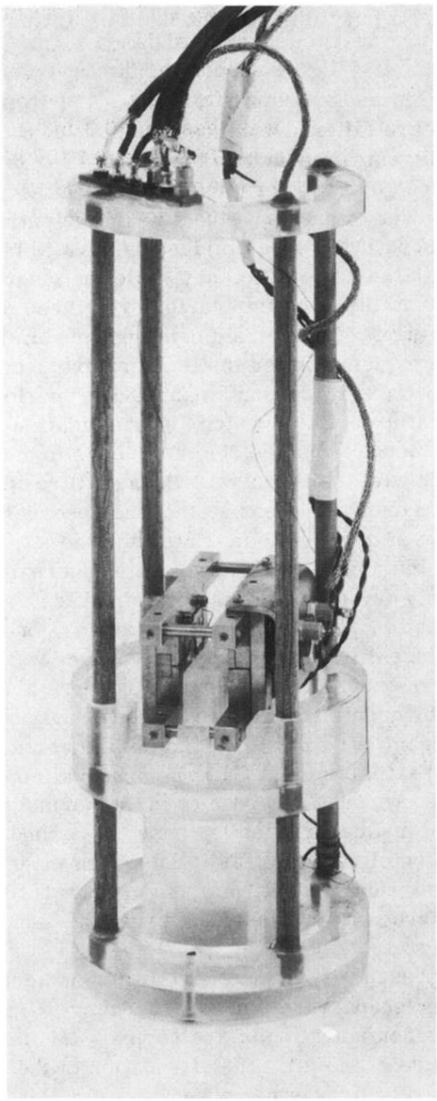

FIG. 5. Assembled counterflow jet and support structure with the second-sound cell.